

MR BO YANG (Orcid ID : 0000-0001-9783-747X)

Article type : Original Article

Using Mesoproterozoic Sedimentary Geochemistry to Reconstruct Basin Tectonic Geography and Link Organic Carbon Productivity to Nutrient Flux from a Northern Australian Large Igneous Province

Bo Yang¹, Alan S. Collins^{1,2}, Grant M. Cox¹, Amber J. M. Jarrett^{2,3}, Steven Denyszyn⁴, Morgan L. Blades¹, Juraj Farkaš¹, Stijn Glorie¹

¹*Tectonics and Earth Systems Research Group, Mawson Centre for Geosciences (MCG), Department of Earth Sciences, The University of Adelaide, SA 5005, Australia.*

²*Mineral Exploration Cooperative Research Centre*

³*Geoscience Australia, GPO Box 378, Canberra, A.C.T., 2601, Australia.*

⁴*School of Earth Sciences, University of Western Australia, Perth, WA, 6009, Australia.*

Abstract

The Beetaloo Sub-basin, northern Australia, is considered the main depocentre of the 1000 km-scale Mesoproterozoic Wilton package of the greater McArthur Basin—the host to one of the oldest hydrocarbon global resources. The *ca.* 1.40–1.31 Ga upper Roper Group and the latest Mesoproterozoic to early Neoproterozoic unnamed group of the Beetaloo Sub-basin, together, record *ca.* 500-million-years of depositional history within the North Australia Craton.

Whole-rock shale Sm–Nd and Pb isotope data from these sediments reveal sedimentary provenance and their evolution from *ca.* 1.35 to 0.85 Ga. Further, these data, together with shale major/trace elements data from this study and pyrolysis data from previous publications, are used to develop a dynamic

This article has been accepted for publication and undergone full peer review but has not been through the copyediting, typesetting, pagination and proofreading process, which may lead to differences between this version and the [Version of Record](#). Please cite this article as [doi: 10.1111/bre.12450](https://doi.org/10.1111/bre.12450)

This article is protected by copyright. All rights reserved

tectonic geography model that links the organic carbon production and burial to an enhanced weathering of nutrients from a large igneous province. The *ca.* 1.35–1.31 Ga Kyalla Formation of the upper Roper Group is composed of isotopically evolved sedimentary detritus that passes up, into more isotopically juvenile Pb values towards the top of the formation. The increase in juvenile compositions coincides with elevated total organic carbon (TOC) contents of these sediments. The coherently enriched juvenile compositions and TOC the upper portions of the Kyalla Formation are interpreted to reflect an increase in nutrient supply associated with the weathering of basaltic sources (e.g. phosphorous). Possible, relatively juvenile, basaltic sources include the Wankanki Supersuite in the western Musgraves and the Derim–Galiwinku large igneous province (LIP). The transition into juvenile, basaltic sources directly before a supersequence-bounding unconformity, is here interpreted to reflect uplift and erosion of the Derim–Galiwinku LIP, rather than an influx of southern, Musgrave sources. A new baddeleyite crystallisation age of 1312.9 ± 0.7 Ma provides both a tight constraint on the age of this LIP, along with its associated magmatic uplift, as well as providing a minimum age constraint for Roper Group deposition. The unconformably overlying lower and upper Jamison sandstones are at least 300 million years younger than the Kyalla Formation and were sourced from the Musgrave Province. An up-section increase in isotopically juvenile compositions seen in these rocks, are interpreted to document the progressive exhumation of the western Musgrave Province. The overlying Hayfield mudstone received detritus from both the Musgrave and Arunta regions, and its isotopic geochemistry reveals affinities with other early Neoproterozoic basins (e.g. Amadeus, Victoria and Officer basins), indicating the potential for inter-basin correlations.

Key Words: North Australia Craton, Beetaloo Sub-basin, Mesoproterozoic to Neoproterozoic shales, Nd and Pb isotopes, tectonic geography, large igneous province, organic carbon enrichment

1. Introduction

The geochemistry of fine-grained sedimentary rocks provides a wealth of information central to interpreting sedimentary processes and reconstructing the tectonic geography of an area, including sediment provenance, sediment transportation pathways, water-rock interaction and organic matter preservation (*Sageman and Lyons, 2003; Brantley et al., 2008; Piper and Calvert, 2009; Cox et al., 2016a*). Theoretically, an integrated understanding of Earth's sedimentary geochemical archive can help elucidate the complex interactions between the climate, biosphere, geography, tectonic evolution, and crust-mantle interactions (e.g. *Anbar and Knoll, 2002; Horton, 2015; Lyons et al., 2015; Cox et al., 2016b; Merdith et al., 2017; Mukherjee et al., 2018*).

The greater McArthur Basin (Close, 2014) of northern Australia is one of the largest and best-preserved archives of Paleo to Mesoproterozoic siliciclastic and biochemical sedimentary successions (i.e. shales and carbonates). The basin covers an area over 145,000 km², forms a temporal record spanning nearly one billion years (from *ca.* 1820 Ma to the early Neoproterozoic), and records the detailed tectonic and sedimentation history of the North Australia Craton (Rawlings, 1999; Ahmad and Munson, 2013; Cox *et al.*, 2016a; Munson, 2016; Munson *et al.*, 2018; Yang *et al.*, 2018, 2019). The subsurface Beetaloo Sub-basin, towards the centre of the greater McArthur Basin, is the depocentre of the upper part of the greater McArthur Basin, represented here by the Roper Group (Lanigan *et al.*, 1994; Ahmad and Munson, 2013) and is the location of on-going hydrocarbon exploration.

This study focuses on the sedimentary geochemistry of the shales, specifically the *ca.* 1.35–1.31 Ga Kyalla Formation of the upper Roper Group and three informally named formations (the lower and upper Jamison sandstones and the Hayfield mudstone) that unconformably overlie the Roper Group and are constrained to be deposited after *ca.* 1.09 Ga and before the Cambrian. We have focussed on these units, to investigate the provenance and tectono-geographic changes at the later stages of deposition within the greater McArthur Basin. Shale whole-rock chemistry and Sm–Nd and Pb isotope data, in combination with new U–Pb isotope dilution thermal ionization mass spectrometry (ID-TIMS) baddeleyite dating of cross-cutting dolerite intrusions, provide a record of the sedimentary history of the basin, as well as a minimum age constraint for deposition. They further reveal the dynamic evolution of the tectonic geography of northern Australia, from the middle Mesoproterozoic to the early Neoproterozoic.

2. Geological Setting

2.1 Roper Group, Kyalla Formation

The greater McArthur Basin covers most of the northern North Australia Craton and it is surrounded by exposed basement areas and orogens (Rawlings, 1999; Ahmad and Munson, 2013; Munson *et al.*, 2016; Munson *et al.*, 2018; Figure 1). The greater McArthur Basin has been sub-divided into five sedimentary packages separated by regional unconformities (Rawlings, 1999; Ahmad and Munson, 2013; Munson *et al.*, 2016; Munson *et al.*, 2018). The Wilton package is the name given to the broad grouping of coeval sedimentary successions deposited in geographically separated basins or sub-basins, including the Roper Group of the McArthur Basin (*sensu strictu*) and the subsurface Beetaloo Sub-basin, the Renner Group of the Tomkinson Province and the Tijunna Group of the Birrindudu Basin (Figure 1; Close, 2014; Munson, 2016; Munson *et al.*, 2018), and potentially the South Nicholson Group of the South Nicholson Basin (Munson, 2016). The Beetaloo Sub-basin is where the thickest succession of these Mesoproterozoic

sediments has been found and is considered to be the depocentre of the Wilton package (*Lanigan et al., 1994; Ahmad and Munson, 2013; Munson, 2016; Munson et al., 2018*). The Beetaloo Sub-basin is divided into the eastern Beetaloo Sub-basin and the western Beetaloo Sub-basin (Figure 1). The eastern portion is the focus of this study. The Roper Group has been sub-divided into two subgroups—the lower Collara Subgroup and the upper Maiwok Subgroup (*Rawlings, 1999; Ahmad and Munson, 2013*). These two subgroups were both deposited in a stable shelf environment (*Abbott and Sweet, 2001; Munson, 2016*). The Collara Subgroup is dominated by sandstones with less voluminous mudrocks, while the Maiwok Subgroup is characterised by fine-grained sedimentary formations with minor sandstones (*Rawlings, 1999; Abbott et al., 2001; Ahmad and Munson, 2013; Munson, 2016; Munson et al., 2018*).

The Kyalla Formation is the uppermost shale-dominated formation of the Maiwok Subgroup in the Beetaloo Sub-basin, and is a principle focus of this research. The Kyalla Formation conformably overlies the Moroak Sandstone and comprises interbedded siltstone and mudstone with minor fine-grained sandstone intervals, and is suggested to have been deposited in a storm-dominated shallow-marine shelf environment (*Abbott et al., 2001; Ahmad and Munson, 2013; Munson, 2016; Munson et al., 2018*). The Kyalla Formation is poorly exposed in the McArthur Basin (mainly in the Urapunga Region), but is well preserved in the subsurface Beetaloo Sub-basin (*Munson, 2016*). The Kyalla Formation has been informally sub-divided into three units (lower, middle and upper members) according to geophysical logs (*Gorter and Grey, 2012; Munson, 2016*). The middle member is slightly coarser-grained (*Gorter and Grey, 2012; Munson, 2016*). The Kyalla Formation contains confirmed hydrocarbon potentials, especially in the lower member, where rocks are prospective for both oil and gas (*Revie, 2017; Munson and Revie, 2018; Revie and Normington, 2018*). The Kyalla Formation exhibits remarkable lateral continuity and thins towards the north–northeast of the eastern Beetaloo Sub-basin (*Munson, 2016; Figure 2*). In the southern and central parts of the basin, the thickness of the Kyalla Formation varies in cores from about 660 m (Elliott-1 – Figure 2) to about 840 m (Shenandoah-1/1A – Figures 1b and 2), whereas in the north, the upper two members are missing and the thickness drops to about 220 m in McManus-1 (Figure 2). The formation is totally missing in Atree-2 (Figure 2). A sandstone interval (informally named the Elliott sandstone member; *Munson et al., 2016*) within the top of the lower Kyalla member can be identified within the south and central parts of the eastern Beetaloo Sub-basin (e.g. cores Elliott-1, Jamison-1, Chanin-1 and Ronald-1; Figure 2), but is absent in the north of the basin (e.g. cores McManus-1 and Atree-2; Figure 2). The absence of this sandstone member in the north is interpreted to suggest its removal by erosion. In the Urapunga Region, the Kyalla Formation shows a variable thickness from ca. 30 m in core Urapunga-4, ca. 52 m in core Scarborough-1 and about 225 m in core Shea-1 (*Munson et al.,*

2016). The maximum depositional age of the Kyalla Formation is constrained to be younger than 1308 ± 41 Ma (2 standard deviations) based on the youngest single-grain detrital zircon age (Yang *et al.*, 2018), while the minimum depositional age is constrained by dolerite sills of the Derim Derim–Galiwinku LIP that cross-cut the Kyalla Formation with a revised age of 1312.9 ± 0.7 Ma (this study). Considering the uncertainties on the above ages, these maximum and minimum depositional age constraints bracket deposition between *ca.* 1349 Ma and 1313 Ma (2 standard deviations). Sandstone samples collected from the Kyalla Formation of the eastern Beetaloo Sub-basin contain detrital zircon age populations and hafnium isotope signatures that are similar to rocks exposed in the Arunta Region, indicating that this formation was sourced from north-flowing rivers from this area (Figure 1; Yang *et al.*, 2018, 2019).

2.2 Latest Mesoproterozoic to Neoproterozoic unnamed group

In the Beetaloo Sub-basin, the Kyalla Formation is unconformably overlain by a set of late Mesoproterozoic to early Neoproterozoic sandstone to mudstone successions comprising three formations/units, informally named the lower Jamison sandstone, the upper Jamison sandstone and the Hayfield mudstone (Munson, 2016). The lower and upper Jamison sandstone units both contain dominantly medium to coarse quartz-lithic sandstone successions with minor siltstone/shale intervals, deposited in a high-energy shoreline to shallow-marine inner shelf setting (Ahmad and Munson, 2013; Lanigan *et al.*, 1994; Munson, 2016; Munson *et al.*, 2018). The Hayfield mudstone conformably overlies the upper Jamison sandstone and is characterised by a set of mudrock-rich organic-poor sediments with minor sandstones, indicative of a subtidal shallow-marine shelf setting (Munson *et al.*, 2018). This mudstone unit is unconformably overlain by a set of late Neoproterozoic to early Cambrian sedimentary basins (e.g. Georgina Basin; Figure 2), as well as by the *ca.* 510 Ma Kalkarindji LIP (Jourdan *et al.*, 2014). The maximum depositional ages for these three formations are constrained by detrital zircon U–Pb isotopic ages, suggesting that the lower Jamison sandstone was deposited after 1092 ± 16 Ma, and the upper Jamison sandstone and Hayfield mudstone were deposited after 959 ± 18 Ma (Yang *et al.*, 2018). The three formations of the unnamed group have been only observed in the Beetaloo Sub-basin. The lower and upper Jamison sandstones show consistent thickness of *ca.* 100 m, whereas significant thickness variations have been observed for the Hayfield mudstone, from ~450m in the central portion of the eastern Beetaloo Sub-basin (e.g. Shenandoah-1/1A—Figure 2), but pinching out towards both the south and north (Figure 2). Detrital zircon U–Pb age and hafnium isotope data collected from these three formations show affinities to those of the Musgrave Province (Figure 1; Munson, 2016; Munson *et al.*, 2018; Yang *et al.*, 2018, 2019).

3. Shale whole-rock chemical composition

3.1 Major/trace elements

A total of twenty-six bulk shale samples were collected from the Kyalla Formation from the core Balmain-1. Samples were collected approximately every 5 meters. Samples were then sent to Bureau Veritas Ltd for further major and trace elements analysis. Detailed sample information, analytical methods and results are presented in the supplementary files.

3.2 Isotopic composition

A total of fifteen bulk shale samples were collected from the core Balmain-1, including five samples from the Kyalla Formation, two samples from the lower Jamison sandstone, one from the upper Jamison sandstone and seven from the Hayfield mudstone. Bulk shale samples for the lower and upper Jamison sandstone were collected from shale-component intervals. Sample information and analytical methods are provided in the supplementary files and the isotope results are presented in Table 1.

Samples from the Kyalla Formation yield whole-rock $\epsilon_{\text{Nd}(t)}$ values ranging from -4.76 to -3.29 (Table 1; Figure 3). Two bulk shale samples from the lower Jamison sandstone yield $\epsilon_{\text{Nd}(t)}$ values of -6.22 and -5.23, showing more evolved characteristics than the sample from the upper Jamison sandstone ($\epsilon_{\text{Nd}(t)}$: -3.63), while $\epsilon_{\text{Nd}(t)}$ values of the samples from the Hayfield mudstone range from -7.83 to -5.09 (Table 1; Figure 3).

The Pb isotopic compositions of the Kyalla Formation are characterised by a large range in $^{206}\text{Pb}/^{204}\text{Pb}$ (13.983 to 16.957), $^{207}\text{Pb}/^{204}\text{Pb}$ (14.276 to 15.766) and $^{208}\text{Pb}/^{204}\text{Pb}$ (35.105 to 39.698) ratios. The samples of the lower Jamison sandstone return $^{206}\text{Pb}/^{204}\text{Pb}$ ratios of 17.207 and 15.886, $^{207}\text{Pb}/^{204}\text{Pb}$ ratios of 15.831 and 15.616, and $^{208}\text{Pb}/^{204}\text{Pb}$ ratios of 40.993 and 39.398. The upper Jamison sample yields a $^{206}\text{Pb}/^{204}\text{Pb}$ ratio of 17.474, a $^{207}\text{Pb}/^{204}\text{Pb}$ ratio of 15.639 and a $^{208}\text{Pb}/^{204}\text{Pb}$ ratio of 41.565. The $^{206}\text{Pb}/^{204}\text{Pb}$ ratios of samples from the Hayfield mudstone range from 15.677 to 17.133, and the $^{207}\text{Pb}/^{204}\text{Pb}$ and $^{208}\text{Pb}/^{204}\text{Pb}$ ratios range from 15.626 to 15.740 and 40.026 to 42.752, respectively (Table 1).

4. Isotope dilution thermal ionization mass spectrometry (ID-TIMS) U–Pb baddeleyite geochronology of the Derim Derim sills

A Derim Derim sill sample (ALT-05) was collected from the core Altree-2 at the depth of 1699 m (Figure 2) for ID-TIMS U–Pb dating. Details of sample and analytical information are provided in the supplementary files and dating results are presented in Table 2.

Six fractions, each of a single baddeleyite crystal, were analysed for U–Pb geochronology after isolation using the Wilfley table (see Supplementary, Figure 4). The grain fragments were generally small (0.1–0.2

μg, calculated from photomicrographs), without any correlation with age or degree of discordance. Calculated U concentrations were between 100 and 200 ppm U, and Th/U ratios were low (~0.1 or lower). All analyses except one (#6) were concordant, with #6 being less than 1% discordant but still resolvably outside of the coherent, concordant grouping of the other data (Figure 4; Table 2). The coherence of the $^{207}\text{Pb}/^{206}\text{Pb}$ dates of all data indicates that any possible Pb loss was recent, and supports our interpretation of the age presented here as the magmatic emplacement age for the sill.

The weighted-mean $^{207}\text{Pb}/^{206}\text{Pb}$ age of all data is 1313.8 ± 1.0 Ma (2SD, MSWD = 0.49, N = 6), while the weighted-mean $^{206}\text{Pb}/^{238}\text{U}$ age of the five concordant analyses is 1312.9 ± 0.7 Ma (2SD, MSWD = 0.88, N = 5). These calculated ages overlap within 2σ uncertainty, though for samples of this age the $^{207}\text{Pb}/^{206}\text{Pb}$ age will always be somewhat older. We consider the weighted-mean $^{206}\text{Pb}/^{238}\text{U}$ age of the coherent cluster of the five concordant analyses to be the most robust determination of the age of the Derim Derim sample.

5. Provenance analysis

5.1 Kyalla Formation

Neodymium isotopic data from five Kyalla Formation mudstone samples overlap with the ϵ_{Nd} evolution trend of the Arunta Region (Figure 3), indicating that this formation might have received detritus from this area. This is consistent with the detrital zircon provenance analysis, which revealed similar zircon U–Pb age and Hf isotope affinities between the Kyalla Formation and the Arunta Region, although the detrital zircon samples were collected from the stratigraphically lower section of this formation (Yang *et al.*, 2018, 2019). Besides that, within the drill hole, a small $\epsilon_{\text{Nd}(t)}$ variation is seen, characterised by an up-section excursion to more positive values, indicative of greater contribution from juvenile sources at the top section of this formation (Figure 5). The positive $\epsilon_{\text{Nd}(t)}$ excursion is mirrored by the covariation in Pb isotopic ratios that show lower radiogenic Pb (^{206}Pb , ^{207}Pb and ^{208}Pb) concentrations at the top of the Kyalla Formation (Figure 5). The Nd and Pb isotope data both support greater contribution from juvenile sources towards the top of the Kyalla Formation. The La/Sm ratio mirrors the Pb isotopic ratios, with an up-section excursion to lower values (Figure 5). This suggests that the juvenile sources are also mafic. This is because, mafic rocks, derived from partial melting of the upper mantle are depleted in light rare-earth elements (LREE), such as La, when compared to felsic rocks that are commonly at least partially derived from melting the continental crust (Winter, 2010). Therefore, more mafic detrital input will lead to lower La/Sm ratios in shales (e.g. Garçon and Chauvel, 2014). The upper Kyalla Formation samples have relative lower La/Sm ratios whereas the other samples from this formation stay closer to the average for the

average upper continental crust (AUCC) value (Figure 5; *Taylor and McLennan, 1995*), suggesting a higher percentage of basaltic-derived components within this part of the formation.

We suggest that the Kyalla Formation was mainly sourced from the Arunta Region, whereas the up-section variation of Nd and Pb isotopes along with La/Sm ratios indicates that the upper Kyalla Formation received detritus from more juvenile basaltic sources. The emergence of juvenile basaltic sources could be conceivably due to a return to the erosion of the Wankanki Supersuite of ca. 1345–1293 Ma plutons in the western Musgrave Province (*Howard et al., 2015*). However, although these are relatively juvenile, they are dominantly granitoids. Alternatively, emplacement of the Derim Derim–Galiwinku LIP is broadly coeval with deposition of the Kyalla Formation and the rocks of this LIP are ubiquitously mafic. The feeder sills and dykes of the Derim Derim–Galiwinku LIP are largely exposed in the Urapunga region in the northeast of the Beetaloo Sub-basin, whereas the relevant volcanic rocks are absent (*Abbott et al., 2001*). We suggest that these volcanic rocks may have been eroded and deposited in the Beetaloo Sub-basin, resulting in a more juvenile, mafic-sourced, component of the uppermost Kyalla Formation.

5.2 Latest Mesoproterozoic to Neoproterozoic group

Whole-rock Sm–Nd isotope analysis shows that three samples, including two from the lower Jamison sandstone and one from the upper Jamison sandstone, plot in the Musgrave Province domain (Figure 3), indicating that they plausibly received detritus from Musgrave Province sources. This is consistent with previous detrital zircon provenance studies that demonstrated significant U–Pb age and Hf isotope similarities between the two sandstone units and the Musgrave Province (*Munson et al., 2016, 2018; Yang et al., 2018, 2019*). Stratigraphically, these three samples show an up-section, more positive, $\epsilon_{\text{Nd}(t)}$ trend (Figure 5), indicating a temporal increase of juvenile material. Potential sources for such juvenile detritus are largely exposed in the western Musgrave Province, in which voluminous juvenile magmas were emplaced during the ca. 1.1 to 1.05 Ga Giles Event (e.g. Warakurna Supersuite; *Wingate et al., 2004; Champion, 2013; Howard et al., 2015*; Figure 4), that occurred during the time represented by the sub-Jamison unconformity. The up-section, more juvenile trend of the lower and upper Jamison sandstone, is interpreted to suggest that the western Musgrave Province progressively became the dominant source for the upper Jamison sandstone, resulting in more juvenile rocks being eroded and then deposited in the Beetaloo Sub-basin.

Compared to the lower and upper Jamison sandstones, the Hayfield mudstone samples yield more negative $\epsilon_{\text{Nd}(t)}$ values, indicating that this formation received detritus from more evolved crustal sources (Figures 3 and 5). In Figure 4, six out of seven samples plot in the overlapping domain of the Musgrave Province and the Arunta Region. Additionally, stratigraphic variations of $\epsilon_{\text{Nd}(t)}$ are seen in this formation,

characterised by an excursion to higher values at the depth of 820m to 770m (Figure 5). The section with higher $\epsilon_{\text{Nd}(t)}$ values is where a sandstone interval (also informally named Hayfield sandstone member; Gorter and Grey, 2013; Munson, 2016) is located (Figure 5). Silverman *et al.* (2007) interpreted this sandstone interval to represent a shallowing event or a period of flood or higher flow rate. Munson *et al.* (2018) presented detrital zircon U–Pb age and Hf isotope data and suggested that this sandstone-rich unit shares significant similarities with the upper and lower Jamison sandstone, indicating they might receive detritus from the same sources (e.g. Musgrave Province). The similarities between this sandstone interval and the underlying sandstone units are further demonstrated here by our Nd isotope data. These show that the two shale samples bounding the sandstone interval, yield similar $\epsilon_{\text{Nd}(t)}$ values to the lower Jamison sandstone samples (Figure 5). We suggest that the Hayfield mudstone probably received detritus from both juvenile sources (e.g. Musgrave Province) and evolved sources (e.g. Arunta Region). Basin-margin progradation, or possibly a major flood event, brought more Musgrave Province detritus into the Beetaloo Sub-basin in middle Hayfield mudstone times.

Provenance analysis illustrates stratigraphic provenance excursion within the lower and upper Jamison sandstones and Hayfield mudstone. The radiogenic Pb profiles of these successions, however, exhibit little variation, especially compared to those seen in the Kyalla Formation (Figure 5). A possible explanation might be that the top section of the Kyalla Formation is being sourced from homogenous juvenile mafic sources (e.g. Derim Derim–Galiwinku LIP). Whereas, the latest Mesoproterozoic to early Neoproterozoic successions received mixed detritus from both juvenile and evolved sources (e.g. Musgrave and Arunta regions). These sources are also likely to be felsic, as established from the La/Sm data, showing that analyses from the lower and upper Jamison sandstones and Hayfield mudstone stay close to the AUC value (Figure 5).

6. Discussion

6.1 Emplacement of the Derim Derim–Galiwinku LIP

The Derim Derim–Galiwinku LIP mafic intrusives are distributed in the northern North Australia Craton from the northern margin of the McArthur Basin (*sensu stricto*) to the northern Beetaloo Sub-basin (Abbott *et al.*, 2001; Ahmad and Munson, 2013; Whelan *et al.*, 2016), and probably extend to the southern Beetaloo Sub-basin, according to geophysical interpretations (Frogtech Geoscience, 2018). The Derim Derim–Galiwinku LIP intrudes the Maiwok Sub-group up to the top of the Kyalla Formation in the Beetaloo Sub-basin and the Bukalorkmi Sandstone in the Urapunga Fault Zone, and is therefore considered to constrain the end of the deposition of the Roper Group (Abbott *et al.*, 2001; Ahmad and

Munson, 2013). The new Derim Derim U–Pb age of 1312.9 ± 0.7 Ma, obtained in this study (Figure 3), is approximately 10 million years younger than previously reported secondary ionization mass spectrometry (SIMS) U–Pb baddeleyite age of 1324 ± 4 Ma (the standard deviation level is unclear as the data are as yet unpublished) from a sill within the Urapunga Fault Zone (*Abbott et al., 2001*). Furthermore, the new date is slightly older than the unnamed dolerite intrusions within the Tomkinson Province, to the south of the Beetaloo Sub-basin that yielded a SIMS $^{207}\text{Pb}/^{206}\text{Pb}$ baddeleyite age of 1295 ± 14 Ma (*Melville, 2010*). In addition, a SIMS $^{207}\text{Pb}/^{206}\text{Pb}$ baddeleyite age of 1329 ± 55 Ma was reported by *Whelan et al. (2016)* from the Galiwinku Dolerite. Although correlations between these mafic intrusions remain unclear, these ages, together, support a period of intraplate mafic magmatism in the North Australian Craton from ca. 1330 to 1295 Ma.

6.2 Uplift of the greater McArthur Basin

The Kyalla Formation represents the final stage of deposition of the Mesoproterozoic Roper Group in the Beetaloo Sub-basin of the greater McArthur Basin. The Beetaloo Sub-basin subsequently experienced a long period (ca. 300 Ma) of erosion and non-deposition, which is reflected by the regional unconformity separating the Kyalla Formation from the post ca. 1090 Ma lower Jamison sandstone (*Yang et al., 2018*). The lateral stratigraphic continuity of the Kyalla Formation suggests that the original extent of this formation was larger than its present distribution (*Munson, 2016*). Besides that, the progressively northward thinning of this formation and the absence of the upper members in the northern Beetaloo Sub-basin suggests that the northern margin of the basin was uplifted into a broad dome and eroded. A possible explanation for this basin uplift could be folding due to a regional compressional event. The Roper Group in the Urapunga Region, north of the major Mallapunyah Fault, was folded at some time after the ca. 1313 Ma Derim Derim intrusions (*Abbott et al., 2001*). However, we suggest that compression is unlikely as an originator of topography that may have been eroded to form the sub-Jamison unconformity, because a) no macroscopic folds are reported from the Beetaloo Basin, and, b) the sub-Jamison unconformity is seen throughout the region, suggesting a broad large wavelength doming to create topography. Intraplate mafic magmatism is also a feature of extensional plume-settings, where such broad domal uplift is expected (*Ernst et al., 2008*). We suggest that the broad upward flexure of the northern Kyalla Formation is associated with magmatic uplift during the emplacement of the Derim Derim–Galiwinku LIP, which progressively inflated the basin from north to south as the plume evolved (Figure 6).

This model explains the change from southerly sources (e.g. Arunta Region) for the majority of the Kyalla Formation to northerly-sourced detritus, from the Derim Derim–Galiwinku LIP, at the top of the formation

(i.e. Urapunga Region; Figure 6a). The subsequent evolution of plume emplacement ultimately resulted in the uplift of the whole Beetaloo Sub-basin resulting in the cessation of deposition within the basin (Figure 6b).

Sedimentary rocks of the Kyalla Formation are also observed, from both core and outcrop, in the Urapunga Region, and show a considerable variation in thickness from a few meters, up to approximately 200 meters (Munson, 2016; Figure 1). We suggest that, during the magmatic uplift, a series of faults may have developed in the Urapunga Region, resulting in Kyalla sediments being deposited within grabens and (or) half-grabens and separated from the Kyalla Formation in the Beetaloo Sub-basin (Figures 6a and 6b). This separation could have resulted in a distinct depositional system in which the overlying Bukalorkmi Sandstone and Chambers River Formation locally developed in the Urapunga Region, but were never deposited in the Beetaloo Sub-basin.

The Derim Derim–Galiwinku magmatism is coeval with the emplacement of the *ca.* 1.33–1.30 Ga Yanliao LIP in the North China Craton (NCC; Zhang *et al.*, 2017). Zhang *et al.* (2017) suggested that the co-occurrence of these intraplate mafic magmatism in both northern Australia and the NCC might indicate that these two cratons were juxtaposed at *ca.* 1.3 Ga. This reconstruction is further supported by the recent palaeomagnetic study revealing that the NAC and NCC were at the similar latitudes at *ca.* 1.3 Ga (Kirscher *et al.*, 2018). The emplacement of the Yanliao diabase sills was accompanied by a significant magmatic uplift that resulted a regional unconformity separating the *ca.* 1.34 Ga Xiamaling Formation and the early Neoproterozoic Qingbaikou Group (Zhang *et al.*, 2017). We suggest that here, in the North Australia Craton, the Roper Group was also uplifted in a similar manner during the Derim Derim–Galiwinku magmatism. The coeval intraplate mafic magmatism and magmatic uplift suggests that the plume head was located between the northern margin of the NAC and north-northeastern margin of the NCC. The plume uplifted both these cratons from their north, simultaneously (Zhang *et al.*, 2017).

6.3 Trigger for organic carbon enrichment

The timing of eruption and erosion of the Derim Derim–Galiwinku LIP coincides with the timing of influx of juvenile basaltic detritus and elevated TOC concentrations at the top section of the Kyalla Formation (Figure 7; Jarrett *et al.*, 2017; Revie and Normington, 2018). The coincidence of an increased basaltic detritus to the weathering flux and elevated TOC is in agreement with many recent studies that have noted mafic rocks, compared to other types of terrestrial rocks, are phosphorous enriched (Horton, 2015). In core Balman-1, the section with more juvenile basaltic compositions contains enriched phosphorous and magnesium, with a smaller increase in calcium—elements that are commonly enriched in basaltic rocks (Figure 8). The weathering of basaltic rocks will deliver more nutrients to sedimentary basins,

compared to typical felsic or granitic rocks, resulting an increase in biological primary productivity (Horton, 2015; Cox *et al.*, 2016a, b).

Provenance analysis in this study shows a geochemical link between mafic volcanism and sedimentation of organic-rich shales. Our hypothesis is that during the rapid weathering of Derim Derim–Galiwinku basaltic rocks, more phosphorus was transported to the Beetaloo Sub-basin than previously (Figures 6a and 8). With increased nutrient delivery, more primary organic matter was generated in the ocean surface waters. Higher primary production would increase the likelihood that more organic matter would be exported to bottom waters and then preserved within the sediments, as seen in upper part of the Kyalla Formation (Figure 7). A similar model has recently been proposed for the underlying hydrocarbon-prone Velkerri Formation (Cox *et al.*, 2016a, 2019; Mukherjee and Large, 2016). The covariance between isotopic ratios, major and trace elements ratios and TOC concentrations within the Kyalla Formation suggests that erosion of the Derim Derim–Galiwinku LIP is likely to be the cause of the TOC enrichment within this formation.

6.4 Early Neoproterozoic tectonic geography

Whole-rock shale Sm–Nd isotope provenance analysis in this study suggests that the two sandstone units of the latest Mesoproterozoic to early Neoproterozoic unnamed group, the lower and upper Jamison sandstones, were sourced from the Musgrave province. We further suggest that the significant up-section, increase in juvenile compositions, may be coeval with the *ca.* 1090 to 1040 Ma Giles event (Howard *et al.*, 2015; Glorie *et al.*, 2017). During the Giles event, voluminous mafic-ultramafic and juvenile felsic rocks were intruded. These were accompanied by widespread volcanism (e.g. Warakurna LIP) and high temperature metamorphism in central Australia (Smithies *et al.*, 2011; Kirkland *et al.*, 2013; Howard *et al.*, 2015). These are mainly exposed in the western Musgrave Province (Figure 9a). The Warakurna LIP has been linked to a deep mantle plume system located beneath the Ngaanyatjarra Rift, in the western Musgrave Province (Wingate *et al.*, 2004). We suggest that the lower Jamison sandstone was predominantly sourced from the central Musgrave Province. During the emplacement of the Warakurna LIP, the western Musgrave gradually uplifted and became the dominant source, thus more juvenile detritus were transported and deposited in the Beetaloo Sub-basin. This resulted in the up-section trend to more juvenile compositions within the lower and upper Jamison sandstone. This provenance variation is also coeval with detrital zircon U–Pb provenance analysis, suggesting that the upper Jamison sandstone samples contain higher proportions of *ca.* 1.1 Ga detrital zircon grains than the lower Jamison sandstone (Munson *et al.*, 2018; Yang *et al.*, 2018). Hafnium isotope analysis shows that these *ca.* 1.1 Ga detrital

zircon grains are juvenile and that many show Pb-loss trends (Yang *et al.*, 2019), which are similar to those from the western Musgrave Province (e.g. Smithies *et al.*, 2011).

We suggest that the fine-grained early Neoproterozoic unit of the unnamed group, the Hayfield mudstone, received mixed detritus from the Musgrave Province and the Arunta Region. This is consistent with the sedimentary formations of the Amadeus Basin in the central Australia. Zhao *et al.* (1992) suggested that the older units in the Amadeus Basin were sourced from the Musgrave Province as well as the Arunta Region according to the whole-rock Sm–Nd data. In the $\epsilon_{\text{Nd}(t)}$ against age plot (Figure 3), analyses from the basal sandstone and mudstone units (the Heavitree Sandstone and Bitter Springs Formation) of the Amadeus Basin all plot in a region overlapping the Musgrave Province and the Arunta Region, similar to those of the Hayfield mudstone, as well as formations from the Officer Basin (Wade *et al.*, 2005). Additionally, Sm–Nd isotopic consistency has also been found in the Auvergne Group of the Victoria Basin in the northwest (Figures 3 and 9a). Carson (2013) presented Sm–Nd isotope data from the Victoria Basin and illustrated a potential connection with the Amadeus Basin. This dataset is also coeval with the latest Mesoproterozoic to early Neoproterozoic unnamed group, indicating a potential connection to the Beetaloo Sub-basin (Figure 9a). The correlations amongst these basins have been further supported by detrital zircon U–Pb data. Consistent detrital zircon U–Pb age spectra, with dominant age populations centred at *ca.* 1.59 Ga and two minor peaks clustered at *ca.* 1.1 Ga and *ca.* 1.77 Ga, have been found among the basal sandstone unit of the Amadeus Basin (Heavitree Sandstone), the basal sandstone unit of the Victoria Basin (Jasper Gorge Sandstone), the Munyu Sandstone of the Murraba Basin and the unnamed group of the Beetaloo Sub-basin (Maidment *et al.*, 2007; Kirkland *et al.*, 2009; Carson, 2013; Haines and Allen, 2016; Munson *et al.*, 2018; Yang *et al.*, 2018; Figure 9b). The potential sources for *ca.* 1.59 Ga and *ca.* 1.1 Ga zircon grains are largely exposed in the Musgrave Province, and those zircon grains with *ca.* 1.77 Ga ages were probably sourced from the Arunta Region (Yang *et al.*, 2018; Figure 9b).

Neoproterozoic central Australia is characterised by the formation of a series of intracontinental sedimentary basins that show considerable stratigraphic similarities, including the Officer, Amadeus, Ngalia and Georgina basins (Figure 9a; Shaw *et al.*, 1991; Zhao *et al.*, 1994). Walter *et al.* (1995) suggested that the sedimentary rocks of these basins are separated remnants from a once-continuous depositional system, the Centralian Superbasin (Figure 9a). Carson (2013) demonstrated that the Victoria Basin might be another correlative of this super basin in the northwest. Further, data collected from the unnamed group in the Beetaloo Sub-basin show consistency with the sedimentary rocks of these basins, suggesting

that the Neoproterozoic Centralian Superbasin probably covered the Beetaloo Sub-basin and is considerably more extensive than previous thought.

7. Conclusions

Stratigraphic variation of shale whole-rock isotopes reveals a dynamic provenance history of the Beetaloo Sub-basin and records *ca.* 500 million years tectonic geography evolution of the North Australia Craton. Further, an integrated analysing of the sedimentary geochemistry data, including data from this research and previously publications, provided a dynamic basin geography model that ties the TOC enrichment to nutrient flux from the Derim Derim–Galiwinku LIP.

We suggest that the Kyalla Formation was mainly sourced from the Arunta Region, whereas the upper section of this formation contains higher juvenile compositions that are interpreted as the weathering of the Derim Derim–Galiwinku LIP. Simultaneously, the weathering of these basaltic rocks also led to higher nutrient levels supplied to the basin, fuelling higher primary production, as shown by the concurrence of more juvenile detritus, phosphorus and TOC enrichment within the upper section of Kyalla Formation. The arrival of the Derim Derim–Galiwinku LIP uplifted the Urapunga Region, and with progressively greater uplift, the whole Beetaloo Sub-basin was exhumed and exposed. The new TIMS U–Pb baddeleyite age of 1312 ± 0.7 Ma (2 standard deviations), for a dolerite sill in the north Beetaloo Sub-basin, provides a new precise age constraint for the age of erosion of the Derim Derim–Galiwinku LIP and interpreted basin uplift event and termination of deposition of the Kyalla Formation as well as the Mesoproterozoic Roper Group.

We suggest that the provenance changed to the Musgrave Province during the deposition of the lower and upper Jamison sandstones. More specifically, the lower Jamison sandstone received detritus from the central Musgrave Province, whereas the western Musgrave Province became the dominant source for the upper Jamison sandstone. This provenance variation is interpreted to be related to the emplacement of Warakurna LIP. The Hayfield mudstone received detritus from both juvenile sources (e.g. Musgrave Province) and evolved sources (e.g. Arunta Region) and share isotopic similarities with the Heavitree–Bitter Springs formations of the Amadeus Basin and the Auvergne Group of the Victoria Basin. The whole-rock geochemical consistency among these early Neoproterozoic basins/strata indicates an extensive super basin with multiple depocentres.

Acknowledgements

This research was funded by an Australian Research Council Linkage Project LP160101353, which is partnered by the Northern Territory Geological Survey, SANTOS Ltd., Origin Energy and Imperial Oil and Gas. David Bruce and Tony Hall are thanked for help collecting geochemical data. AJMJ publishes with the permission of the CEO, Geoscience Australia. This manuscript is a contribution to IGCP Projects 628 (Gondwana Map) and #648 (Supercontinents and Earth Evolution). ASC, JF and AJMJ are supported by the Mineral Exploration Cooperative Research Centre whose activities are funded by the Australian Government's Cooperative Research Centre Programme. This is MinEx CRC Document 2020/5. M. Orr, J. Mulder, C. Kirkland, C. Verdel and an unnamed reviewer are acknowledged and thanked for their constructive comments, which greatly improved the paper.

Data Availability Statement

The data that support the findings of this study are openly available in <https://geoscience.nt.gov.au/gemis/ntgsjspui/handle/1/86287>, (Jarrett, et al., 2017).

The data that support the findings of this study are openly available in <https://geoscience.nt.gov.au/gemis/ntgsjspui/handle/1/82595>, (Revie, D., Normington, V., 2018).

References

- Abbott, S. T. & Sweet, I. P. (2000). Tectonic control on third-order sequences in a siliciclastic ramp-style basin: An example from the Roper Superbasin (Mesoproterozoic), northern Australia. *Australian Journal of Earth Sciences*, **47**(3), 637-657. <https://doi.org/10.1046/j.1440-0952.2000.00795.x>
- Abbott, S. T., Sweet, I. P., Plumb, K. A., Young, D. N., Cutovinos, A., Ferenczi, P. A. & Pietsch, B. A. (2001). *Roper Region: Urapunga and Roper River Special, Northern Territory (Second Edition; 1:250 000 geological map series explanatory notes)*. Northern Territory Geological Survey and Geoscience Australia. <https://geoscience.nt.gov.au/gemis/ntgsjspui/handle/1/81859>
- Ahmad, M. & Munson, T. J. (2013). *Northern Territory Geological Survey, Geology and mineral resources of the Northern Territory, Special Publication 5*. Northern Territory Geological Survey. <https://geoscience.nt.gov.au/gemis/ntgsjspui/handle/1/81446>
- Anbar, A. D. & Knoll, A. H. (2002). Proterozoic ocean chemistry and evolution: a bioinorganic bridge? *Science*, **297**(5584), 1137-42. <https://doi.org/10.1126/science.1069651>
- Betts, P., Armit R. & Ailleres, L. (2015). Potential-field interpretation mapping of the greater McArthur Basin. PGN Geoscience Report 15/2014: in Geophysical and structural interpretation of the greater McArthur Basin.

<https://geoscience.nt.gov.au/gemis/ntgsjspui/handle/1/81754>

Brantley, S. L., Kubicki, J. D. & White, A. F. (2008). Kinetics of water-rock interaction. *Springer, New York*.

<https://doi.org/10.1007/978-0-387-73563-4>

Carson, C. J. (2013). The Victoria and Birrindudu Basins, Victoria River Region, Northern Territory, Australia: a SHRIMP U–Pb detrital zircon and Sm–Nd study. *Journal of the Geological Society of Australia*, **60(2)**, 175–196.

<https://doi.org/10.1080/08120099.2013.772920>

Champion, D. C. (2013). Neodymium depleted mantle model age map of Australia: explanatory notes and user guide.

Geoscience Australia, Record 2013/44. <https://doi.org/10.11636/Record.2013.044>

Close, D. F. (2014). The McArthur Basin: NTGS' approach to a frontier petroleum basin with known base metal prospectivity. *Annual Geoscience Exploration Seminar (AGES) Proceedings*.

<https://geoscience.nt.gov.au/gemis/ntgsjspui/handle/1/82357>

Cox, G. M., Jarrett, A., Edwards, D., Crockford, P. W., Halverson, G. P., Collins, A. S., Poirier, A. and Li, Z. X. (2016a). Basin redox and primary productivity within the Mesoproterozoic Roper Seaway. *Chemical Geology*, **440**, 101–114. <https://doi.org/10.1016/j.chemgeo.2016.06.025>

Cox, G. M., Halverson, G. P., Stevenson, R. K., Vokaty, M., Poirier, A., Kunzmann, M., Li, Z. X., Denyszyn, S. W., Strauss, J. V. and Macdonald, F. A. (2016b). Continental flood basalt weathering as a trigger for Neoproterozoic snowball earth. *Earth & Planetary Science Letters*, **446**, 89–99. <https://doi.org/10.1016/j.epsl.2016.04.016>

Cox, G. M., Sansjofre, P., Blades, M. L., Farkas, J. & Collins, A. S. (2019). Dynamic interaction between basin redox and the biogeochemical nitrogen cycle in an unconventional Proterozoic petroleum system. *Scientific Reports*, 9:5200. <https://doi.org/10.1038/s41598-019-40783-4>

Ernst, R. E., Wingate, M. T. D., Buchan, K. L. & Li, Z. X. (2008). Global record of 1600–700 Ma Large Igneous Provinces (LIPS): Implications for the reconstruction of the proposed Nuna (Columbia) and Rodinia supercontinents. *Precambrian Research*, **160(1)**, 159–178. <https://doi.org/10.1016/j.precamres.2007.04.019>

Edgoose, C. J., Scrimgeour, I. R. & Close, D. F. (2004). Geology of the Musgrave Block, Northern Territory. *Northern Territory Geological Survey, Report 15*. <https://geoscience.nt.gov.au/gemis/ntgsjspui/handle/1/81551>

Frogtech Geoscience (2018). SEEBASE® study and GIS for greater McArthur Basin. *Northern Territory Geological Survey, Digital Information Package DIP 017*. <https://geoscience.nt.gov.au/gemis/ntgsjspui/handle/1/87064>

Garçon, M. & Chauvel, C. (2014). Where is basalt in river sediments, and why does it matter?. *Earth & Planetary Science Letters*, **407**, 61–69. <https://doi.org/10.1016/j.epsl.2014.09.033>

Glorie, S., Agostino, K., Dutch, R., Pawley, M., Hall, J., Danišik, M., Evans, N. J. & Collins, A. S. (2017). Thermal history and differential exhumation across the eastern Musgrave Province, South Australia: insights from low-temperature thermochronology. *Tectonophysics*, **703–704**, 23–41, <https://doi.org/10.1016/j.tecto.2017.03.003>

Gorter, J. D. & Grey, K. (2013). Middle Proterozoic biostratigraphy and log correlations of the Kyalla and Chambers River Formations Beetaloo Sub-basin, Northern Territory, Australia. In *West Australian Basins Symposium (WABS) III. Poster*. Petroleum Exploration Society of Australia.

- Haines, P. W. & Allen, H. J. (2016). The Murraba Basin: another piece of the Centralian Superbasin jigsaw puzzle falls into place. *GSWA 2016 extended abstracts: promoting the prospectivity of Western Australia*. <https://geodocs.dmirs.wa.gov.au/Web/documentlist/3/Combined/N15DC%2F9>
- Horton, F. (2015). Did phosphorus derived from the weathering of Large Igneous Provinces fertilize the Neoproterozoic ocean?. *Geochemistry Geophysics Geosystems*, **16(6)**, 1723-1738. <https://doi.org/10.1002/2015GC005792>
- Howard, H. M., Smithies, R. H., Kirkland, C. L., Kelsey, D. E., Aitken, A., Wingate, M. T. D., Quentin de Gromard, R., Spaggiari, C. V. & Maier, W.D. (2015). The burning heart — the Proterozoic geology and geological evolution of the west Musgrave Region, central Australia. *Gondwana Research*, **27(1)**, 64-94. <https://doi.org/10.1016/j.gr.2014.09.001>
- Jarrett, A. J. M., Edwards, D. S., Hong, Z., Palatty, P., Byass, J. & Webster, T. (2017). Geochemistry of drillcore Balmain 1, Beetaloo Sub-basin, McArthur Basin, NT. *Geoscience Australia, Record*, 2017-001. <https://geoscience.nt.gov.au/gemis/ntgsjspui/handle/1/86287>
- Jourdan, F., Hodges, K., Sell, B., Schaltegger, U., Wingate, M. T. D., Evins, L. Z., Söderlund, U., Haines, P. W., Phillips, D. & Blenkinsop, T. (2014). High-precision dating of the Kalkarindji large igneous province, Australia, and synchrony with the Early-Middle Cambrian (Stage 4-5) extinction. *Geology*, **42(6)**, 543-546. <https://doi.org/10.1130/G35434.1>
- Kirkland, C. L., Wingate, M. T. D., Spaggiari C. V. & Tyler I. M. (2009).184339: sandstone, Pollock Hills. *Geochronology Record* 817. *Geological Survey of Western Australia, Record* 2011/4.
- Kirkland, C. L., Smithies, R. H., Woodhouse, A. J., Howard, H. M., Wingate, M. T. D., Belousova, E. A., Cliff, J. B., Murphy, R. C. & Spaggiari, C. V. (2013). Constraints and deception in the isotopic record; the crustal evolution of the west Musgrave Province, central Australia. *Gondwana Research*, **23(2)**, 759-781. <https://doi.org/10.1016/j.gr.2012.06.001>
- Kirscher, U., Mitchell, R., Liu, Y., Li, Z. X., Cox, G. M., Nordsvan, A., Wang, C. & Pisarevsky, S. (2018). Long lived supercontinent Nuna - updated paleomagnetic constraints from Australia. 2018, *AGU Fall Meeting* (abstract #GP21B-0647)
- Lanigan, K., Hibbird, S., Menpes, S. & Torkinton, J. (1994). Petroleum exploration in the Proterozoic Beetaloo sub-basin, Northern Territory. *APEA JOURNAL*, **34**, 674-674. <https://doi.org/10.1071/AJ93050>
- Lyons, T. W., Reinhard, C. T. & Planavsky, N. J. (2015). The rise of oxygen in earth's early ocean and atmosphere. *Nature*, **506(7488)**, 307-315. <https://doi.org/10.1038/nature13068>
- Maidment, D. W., Williams, I. S. & Hand, M. (2010). Testing long-term patterns of basin sedimentation by detrital zircon geochronology, Centralian Superbasin, Australia. *Basin Research*, **19(3)**, 335-360. <https://doi.org/10.1111/j.1365-2117.2007.00326.x>
- Melville, P. M. (2010). Geophysics and drilling collaboration final report for drilling program, Lake Woods Project, EL23687, EL24520, EL25631, EL27317, EL27318. *Northern Territory Geological Survey, Open File Report* CR2010-0226. <https://geoscience.nt.gov.au/gemis/ntgsjspui/handle/1/75769>

- Merdith, A. S., Collins, A. S., Williams, S. E., Pisarevsky, S., Foden, J. F., Archibald, D., Blades, M. L., Alessio, B. L., Armistead, S., Plavsa, D., Clark, C. & Müller, R. D. (2017). A full-plate global reconstruction of the Neoproterozoic. *Gondwana Research*, **50**, 84-134. <https://doi.org/10.1016/j.gr.2017.04.001>
- Mukherjee I. & Large, R. R. (2016). Pyrite trace element chemistry of the Velkerri Formation, Roper Group, McArthur Basin: Evidence for atmospheric oxygenation during the Boring Billion. *Precambrian Research*. **281**, 13-26. <https://doi.org/10.1016/j.precamres.2016.05.003>
- Mukherjee I., Large, R. R., Corkrey, R. & Danyushevsky, L. V. (2018). The Boring Billion, a slingshot for Complex Life on Earth. *Scientific Reports*, 8:4432. <https://doi.org/10.1038/s41598-018-22695-x>
- Munson, T. J, Kruse, P. D. & Ahmad, M. (2013). Chapter 22 Centralian Superbasin, in Ahmad, M. & Munson, T. J. (Eds.), *Geology and mineral resources of the Northern Territory* (Special Publication 5, p. 22.1–22.19). Northern Territory Geological Survey. <https://geoscience.nt.gov.au/gemis/ntgsjspui/handle/1/81502>
- Munson, T. J. (2016). Sedimentary characterisation of the Wilton package, greater McArthur Basin. Northern Territory. *Northern Territory Geological Survey, Record 2016-003*. <https://geoscience.nt.gov.au/gemis/ntgsjspui/handle/1/82741>
- Munson, T.J. & Revie, D. (2018). Stratigraphic subdivision of Velkerri Formation, Roper Group, McArthur Basin, Northern Territory. *Northern Territory Geological Survey, Record 2018-006*. <https://geoscience.nt.gov.au/gemis/ntgsjspui/handle/1/87322>
- Munson, T. J, Thompson, J. M, Zhukova, I., Meffre, S., Beyer, E. E., Woodhead, J. D. & Whelan, J. A. (2018). Summary of results. NTGS laser ablation ICP-MS U–Pb and Lu–Hf geochronology project: Roper Group and overlying ungrouped units (McArthur Basin), Renner Group (Tomkinson Province), Tjunna Group (Birringdudu Basin). *Northern Territory Geological Survey, Record 2018-007*. <https://geoscience.nt.gov.au/gemis/ntgsjspui/handle/1/87656>
- Piper, D. Z. & Calvert, S. E. (2009). A marine biogeochemical perspective on black shale deposition. *Earth Science Reviews*, **95(1–2)**, 63-96. <https://doi.org/10.1016/j.earscirev.2009.03.001>
- Rawlings, D. J. (1999). Stratigraphic resolution of a multiphase intracratonic basin system: The McArthur Basin, northern Australia. *Australian Journal of Earth Sciences*, **46(5)**, 703-723. <https://doi.org/10.1046/j.1440-0952.1999.00739.x>
- Revie, D. (2017). Volumetric resource assessment of the lower Kyalla and middle Velkerri formations of the McArthur Basin. *Annual Geoscience Exploration Seminar (AGES) Proceedings, Alice Springs, Northern Territory 28–29 March 2017*. <https://geoscience.nt.gov.au/gemis/ntgsjspui/handle/1/85107>
- Revie, D. & Normington, V. (2018). Shale resource data from the greater McArthur Basin. *Northern Territory Geological Survey, Digital Information Package DIP 014*. <https://geoscience.nt.gov.au/gemis/ntgsjspui/handle/1/82595>
- Sageman, B. B. & Lyons, T. W. (2003). Geochemistry of fine-grained sediments and sedimentary rocks. *Treatise on Geochemistry*, **7**, 115-158. <https://doi.org/10.1016/B0-08-043751-6/07157-7>

- Shaw, R. D. (1991). The tectonic development of the Amadeus Basin, central Australia. In: Korsch, R. J. & Kennard, J. M. (Eds.), *Geological and Geophysical Studies in the Amadeus Basin, Central Australia* (pp.429–461). Bureau of Mineral Resources, Australia. <https://ecat.ga.gov.au/geonetwork/srv/eng/catalog.search#/metadata/33>
- Silverman, M. R., Landon, S. M., Leaver, J. S., Mather, T. J. & Berg, E. (2007). No fuel like an old fuel: Proterozoic oil and gas potential in the Beetaloo Basin, Northern Territory, Australia: in Munson, T. J. & Ambrose, G. J. (Eds.), *In Proceedings of the Central Australian Basins Symposium (CABS) Northern Territory Geological Survey, Special Publication* (Vol. 2). Northern Territory Geological Survey.
- Smithies, R. H., Howard, H. M., Evins, P. M., Kirkland, C. L., Kelsey, D. E., Hand, M., Wingate, M. T. D., Collins, A. S., Belousova, E. & Allchurch, S. (2010). Geochemistry, geochronology, and petrogenesis of Mesoproterozoic felsic rocks in the west Musgrave Province, central Australia, and implications for the Mesoproterozoic tectonic evolution of the region. *Geological Survey of Western Australia, Report 106*.
- Smithies, R. H., Howard, H. M., Evins, P. M., Kirkland, C. L., Kelsey, D. E., Hand, M., Wingate, M. T. D., Collins, A. S. & Belousova, E. A. (2011). High-temperature granite magmatism, crust–mantle interaction and the Mesoproterozoic intracontinental evolution of the Musgrave Province, central, Australia. *Journal of Petrology*, **52**(5), 931-958. <https://doi.org/10.1093/petrology/egr010>
- Sun, S. S. & McDonough, W. F. (1989). Chemical and isotopic systematics of oceanic basalts: implications for mantle composition and processes. *Geological Society London Special Publications*, **42**(1), 314-345. <https://doi.org/10.1144/GSL.SP.1989.042.01.19>
- Taylor, S. R. & McLennan, S. M. (1995). The geochemical evolution of the continental crust. *Reviews of Geophysics*, **33**(2), 241-265. <https://doi.org/10.1029/95RG00262>
- Wade, B. P. (2005). Nd isotopic and geochemical constraints on provenance of sedimentary rocks in the eastern Officer Basin, Australia: implications. *Journal of Geological Society London*, **162**, 513-530. <https://doi.org/10.1144/0016-764904-001>
- Wade, B.P., Kelsey, D.E., Hand, M., Barovich, K.M., 2008. The Musgrave Province: stitching north, west and south Australia. *Precambrian Research*, **166**(1), 370-386. <https://doi.org/10.1016/j.precamres.2007.05.007>
- Walter, M. R., Veevers, J. J., Calver, C. R. & Grey, K. (1995). Neoproterozoic stratigraphy of the Centralian Superbasin, Australia. *Precambrian Research*, **73**(1–4), 173-195. [https://doi.org/10.1016/0301-9268\(94\)00077-5](https://doi.org/10.1016/0301-9268(94)00077-5)
- Whelan, J. A., Beyer, E. E., Donnellan, N., Bleeker, W., Chamberlin, K. R., Soderlund, U. & Ernst, R. E. (2016). 1.4 billion years of Northern Territory geology: Insights from collaborative U–Pb zircon and baddeleyite dating. *Annual Geoscience Exploration Seminar (AGES) Proceedings*. <https://geoscience.nt.gov.au/gemis/ntgsjspui/handle/1/82750>
- Wingate, M. T. D., Pirajno, F. & Morris, P. A. (2004). Warakurna large igneous province: a new Mesoproterozoic large igneous province in west-central Australia. *Geology*, **32**(2), 105-108. <https://doi.org/10.1130/G20171.1>
- Winter, J. D. (2010). Principles of igneous and metamorphic petrology (2nd ed.). *New York: Prentice Hall*.
- Yang, B., Smith, T. M., Collins, A. S., Munson, T. J., Schoemaker, B., Nicholls, D., Cox, G., Farkas, J. & Glorie, S. (2018). Spatial and temporal detrital zircon U–Pb provenance of the hydrocarbon-bearing upper Roper Group, Beetaloo

<https://doi.org/10.1016/j.precamres.2017.10.025>

Yang, B., Collins, A. S., Blades, M. L., Capogreco, N., Payne, J. L., Munson, T. J., Cox, G. M. & Glorie, S. (2019). Middle-late Mesoproterozoic tectonic geography of the North Australia Craton: U–Pb and Hf isotopes of detrital zircons in the Beetaloo Sub-basin, Northern Territory, Australia. *Journal of the Geological Society, London*. <https://doi.org/10.1144/jgs2018-159>

Zhang, S. H., Zhao, Y., Li, X. H., Ernst, R. E. & Yang, Z. Y. (2017). The 1.33–1.30 Ga Yanliao large igneous province in the North China Craton: Implications for reconstruction of the Nuna (Columbia) supercontinent, and specifically with the North Australian Craton. *Earth and Planetary Science Letters*, **465**, 122–125. <https://doi.org/10.1016/j.epsl.2017.02.034>

Zhao, J. X., McCulloch, M. T. & Bennett, V. C. (1992). Sm–Nd and U–Pb zircon isotopic constraints on the provenance of sediments from the Amadeus Basin, central Australia: evidence for REE fractionation. *Geochimica Et Cosmochimica Acta*, **56**(3), 921-940. [https://doi.org/10.1016/00167037\(92\)90037-J](https://doi.org/10.1016/00167037(92)90037-J)

Zhao, J. X., McCulloch, M. T. & Korsch, R. J. (1994). Characterisation of a plume-related ~ 800 Ma magmatic event and its implications for basin formation in central-southern Australia. *Earth & Planetary Science Letters*, **121**(3–4), 349-367. [https://doi.org/10.1016/0012-821X\(94\)90077-9](https://doi.org/10.1016/0012-821X(94)90077-9)

Captions

Figure 1 Map showing the extent of the Beetaloo Sub-basin and locations of analysed drill holes (SEEBASE™ basement surface image after *Frogtech Geoscience (2018)*) modified after *Munson (2016)* and *Betts et al. (2015)*. Note the locations of Balmian-1 and Shenandoah-1A are overlapped in the map due to their close distance.

Figure 2 Beetaloo Sub-basin N–S fence diagram with gamma-ray (GR) logs. The Kyalla Formation thins towards the north, which is interpreted to be due to progressive increased pre-Jamison sandstone uplift and erosion towards the north (modified after *Gorter and Grey, 2013*).

Figure 3 Shale whole-rock $\epsilon_{\text{Nd}(t)}$ vs age diagram illustrating potential provenance regions. Published individual Nd analyses from potential provenance areas (e.g. Musgrave Province and Arunta Region) are from *Champion (2013) and references therein*. The $\epsilon_{\text{Nd}(t)}$ evolution curve of the Arunta Region was plotted according to an assumed continental crust value of $^{147}\text{Sm}/^{144}\text{Nd} = 0.11$, following *Champion (2013)*, and the range of this curve is constrained by two standard deviation intervals of the kernel density distributed T_{DM} data from *Champion (2013) and references therein*. The Musgrave Province $\epsilon_{\text{Nd}(t)}$ evolution trend is plotted after *Smithies et al. (2013)*. *Data of Black Point Sandstone and Auvergne Group (Victoria Basin) are from *Carson (2013)*. **Data of Amadeus Basin (Heavitree Sandstone, Bitter Springs Formation and Areyonga Formation) are from *Zhao et al. (1994)*. ***Data of Officer Basin are from *Wade et al. (2005)*. CHUR: chondrite reservoir.

Figure 4 TIMS U–Pb baddeleyite concordia plot of the dolerite sample collected from Altree-2 borehole at a depth of 1699m.

Figure 5 Stratigraphy versus chemistry diagrams in borehole Balmain-1 illustrating the up-section variation of selected isotopes and trace element ratios. Average upper continental crust (AUCC) values from *Taylor and McLennan (1995)*. Mid-ocean ridge basalt (MORB) data from *Sun and McDonough (1989)*. Trace elements data from *Jarrett et al. (2017)*. All uncertainties are presented at 2σ level and most of them are smaller than the plotted points.

Figure 6 Simplified geographic cartoon showing the envisaged paleogeography during the emplacement of the Derim Derim–Galiwinku LIP: (a) the weathering of the Derim Derim–Galiwinku LIP transported more phosphorus to the basin, which enhanced primary production in the ocean surface waters and resulted in organic carbon enrichment in the sediments; (b) the basin was uplifted from the north during continued plume-related uplift, resulting in the Kyalla Formation being preferentially eroded towards to the north.

Figure 7 Stratigraphic-Total Organic Carbon (TOC) plots illustrating TOC enrichment in the upper section of the Kyalla Formation. The upper parts of the Kyalla Formation are interpreted to have been eroded from Chanin-1, Ronald-1 and McManus-1. The TOC enrichment is absent in the upper Kyalla Formation from Elliott-1, which is interpreted to reflect erosion during post deposition fault activities. TOC data from *Revie and Normington (2018)* and *Jarrett et al. (2017)*.

Figure 8 Stratigraphic- major elements plot illustrating the juvenile detritus enriched section is consistent higher component of elements that are enriched in basaltic rocks.

Figure 9 (a) Geological map showing the distribution of Neoproterozoic basins within Australia; (b) Detrital zircon U–Pb age kernel density distribution plots illustrating the provenance consistency among the Jasper Gorge Sandstone (Victoria Basin), Munyu sandstone (Murraba Basin), Heavitree Sandstone (Amadeus Basin), lower and upper Jamison sandstone and Hayfield mudstone (Beetaloo Sub-basin), and their interpreted provenances (Arunta Region and Musgrave Province). Detrital zircon U–Pb age data are from *Maidment et al. (2007)*, *Kirkland et al. (2009)*, *Carson (2013)*, *Haines and Allen (2016)*, *Munson et al. (2018)*, *Yang et al. (2018 and references therein)*.

Table 1 Sm–Nd and Pb-isotopic compositions of the analysed formations from the core Balmain-1.

Table 2 U–Pb isotopic data (one crystal per fraction) for baddeleyite from the Derim Derim sills (sample ALT-05). * Pbc = Total common Pb including analytical blank (0.8 ± 0.3 pg per analysis). ρ = error correlation coefficient of radiogenic $^{207}\text{Pb}/^{235}\text{U}$ vs. $^{206}\text{Pb}/^{238}\text{U}$. All uncertainties given at 2σ .

Table 1 Sm–Nd and Pb-isotopic compositions of the analysed formations from the core Balmain-1.

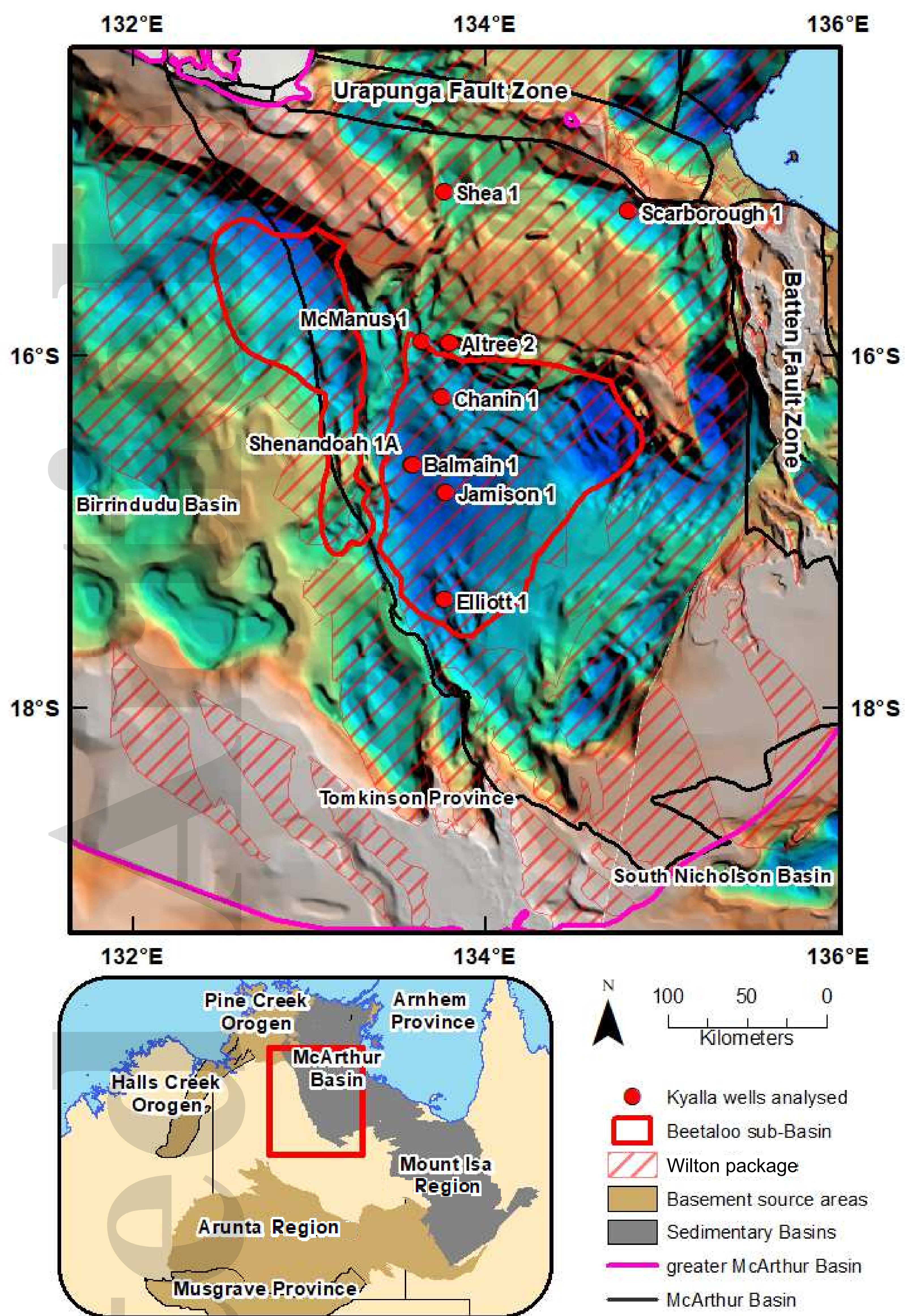
Formation	Sample	Depth (m)	Age (Ma)	Nd (ppm)	Sm (ppm)	$^{143}\text{Nd}/^{144}\text{Nd}(\text{t})$	$\epsilon_{\text{Nd}(\text{t})}$	2s.e	T_{DM} (Ga)	$^{206}\text{Pb}/^{204}\text{Pb}$	2s.e	$^{207}\text{Pb}/^{204}\text{Pb}$	2s.e	$^{208}\text{Pb}/^{204}\text{Pb}$	2s.e
Hayfield mudstone	Bal-by-15	646	950	52.287	0.195	0.511087	-6.38	0.05	2.09	16.594	0.106	15.688	0.113	40.026	0.119
	Bal-by-14	675	950	60.726	0.188	0.511099	-6.14	0.06	2.02	16.173	0.049	15.631	0.050	40.156	0.049
	Bal-by-13	706	950	36.155	0.176	0.511121	-5.71	0.05	1.92	17.026	0.051	15.723	0.064	40.571	0.083
	Bal-by-12	746	950	56.289	0.200	0.511106	-6.89	0.04	2.16	17.133	0.194	15.740	0.204	42.204	0.204
	Bal-by-11	775	950	45.492	0.186	0.511131	-5.51	0.03	1.96	15.677	0.104	15.707	0.107	42.752	0.109
	Bal-by-10	807	950	73.866	0.177	0.511152	-5.09	0.05	1.88	17.010	0.127	15.626	0.128	42.317	0.131
	Bal-by-9	838	950	37.016	0.218	0.511013	-7.83	0.04	2.41	16.889	0.006	15.659	0.005	41.518	0.005
upper Jamison sandstone	Bal-by-8	869	950	34.217	0.202	0.511227	-3.63	0.08	1.93	17.474	0.174	15.639	0.177	41.565	0.171
lower Jamison sandstone	Bal-by-7	888	950	79.571	0.191	0.511145	-5.23	0.05	2.06	15.886	0.117	15.616	0.124	39.398	0.123
	Bal-by-6	911	950	121.63	0.204	0.511094	-6.22	0.04	2.15	17.207	0.078	15.831	0.079	40.993	0.074
Kyalla Fm.	Bal-by-5	940	1320	61.016	0.233	0.510713	-4.31	0.05	2.51	13.983	0.020	15.205	0.021	37.300	0.023
	Bal-by-4	953	1320	43.914	0.171	0.510765	-3.29	0.05	2.03	14.253	0.415	14.276	0.356	35.105	0.415
	Bal-by-3	985	1320	52.200	0.197	0.510691	-4.74	0.05	2.27	16.957	0.061	15.766	0.072	39.698	0.086
	Bal-by-2	1016	1320	44.967	0.197	0.51069	-4.76	0.05	2.27	16.083	0.034	15.712	0.036	39.400	0.036
	Bal-by-1	1050	1320	53.686	0.192	0.51073	-3.98	0.05	2.18	16.121	0.043	15.676	0.048	39.090	0.053

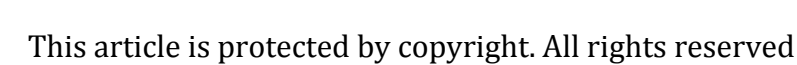
Table 2: U–Pb isotopic data (one crystal per fraction) for baddeleyite from the Derim Derim sills (sample ALT-05).

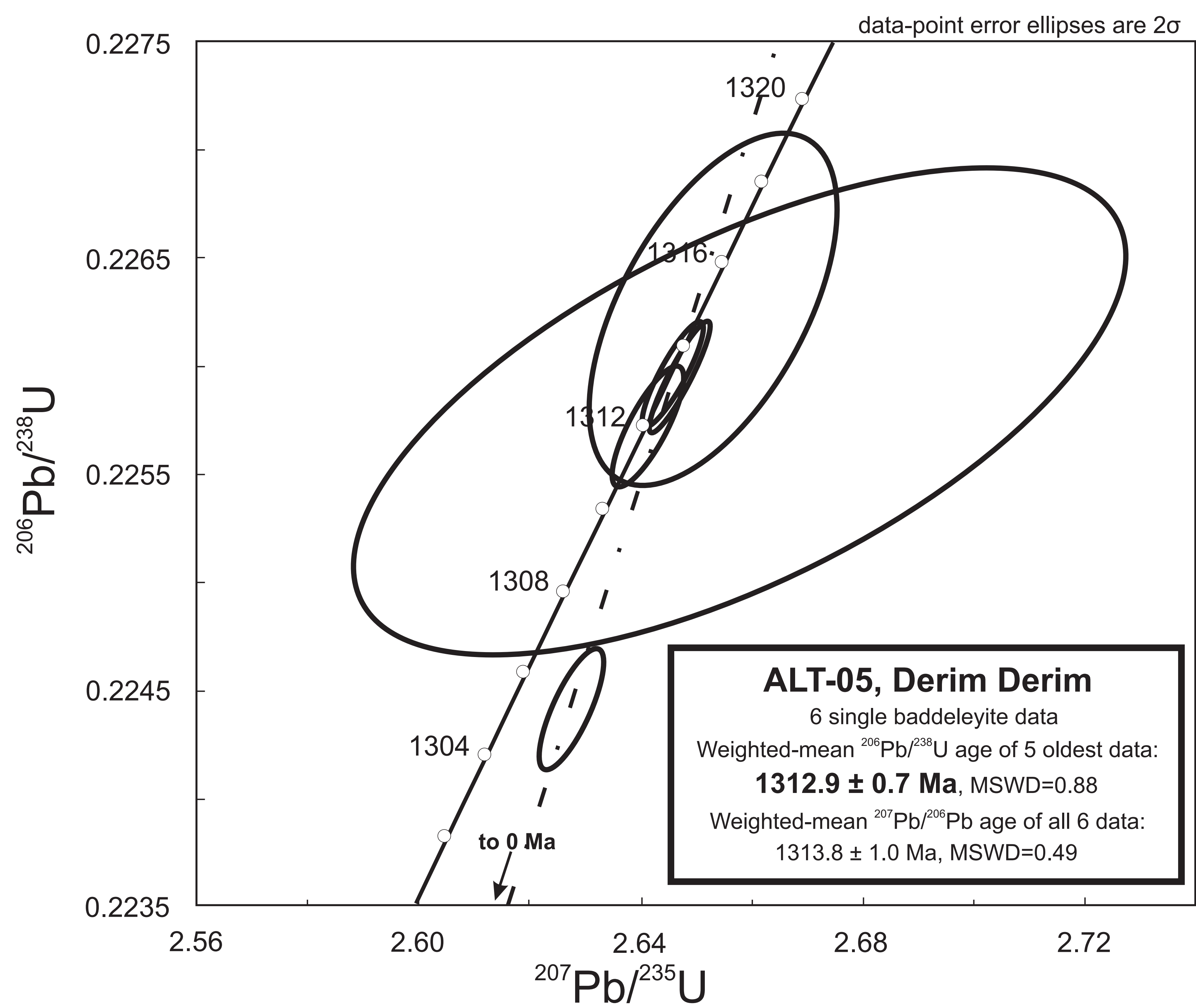
Sample	Wt.	U	Pb _c	mol%	Th	²⁰⁶ Pb	²⁰⁷ Pb	±	²⁰⁷ Pb	±	²⁰⁶ Pb	±	ρ	²⁰⁶ Pb/ ²³⁸ U	±	²⁰⁷ Pb/ ²⁰⁶ Pb	±
	(μg)	(ppm)	(pg)	Pb*	U	²⁰⁴ Pb	²⁰⁶ Pb	(%)	²³⁵ U	(%)	²³⁸ U	(%)		Age (Ma)	(Ma)	Age (Ma)	(Ma)
1	0.1	118	0.2	85	0.03	122	0.08503	0.58	2.6528	0.70	0.226262	0.29	.58	1314.88	3.85	1316	11.3
2	0.2	109	0.2	99	0.12	1181	0.08496	0.09	2.6468	0.17	0.225953	0.09	.92	1313.25	1.23	1315	1.8
3	0.2	196	0.2	98	0.06	1133	0.08492	0.10	2.6455	0.17	0.225949	0.09	.89	1313.23	1.22	1314	1.9
4	0.1	115	0.3	77	0.08	71	0.08537	1.89	2.6578	2.12	0.225794	0.41	.64	1312.42	5.37	1324	36.6
5	0.2	151	0.2	98	0.07	610	0.08487	0.12	2.6414	0.18	0.225718	0.10	.80	1312.02	1.32	1313	2.3
6	0.1	196	0.2	97	0.06	592	0.08491	0.12	2.6274	0.19	0.224415	0.10	.79	1305.16	1.33	1314	2.4

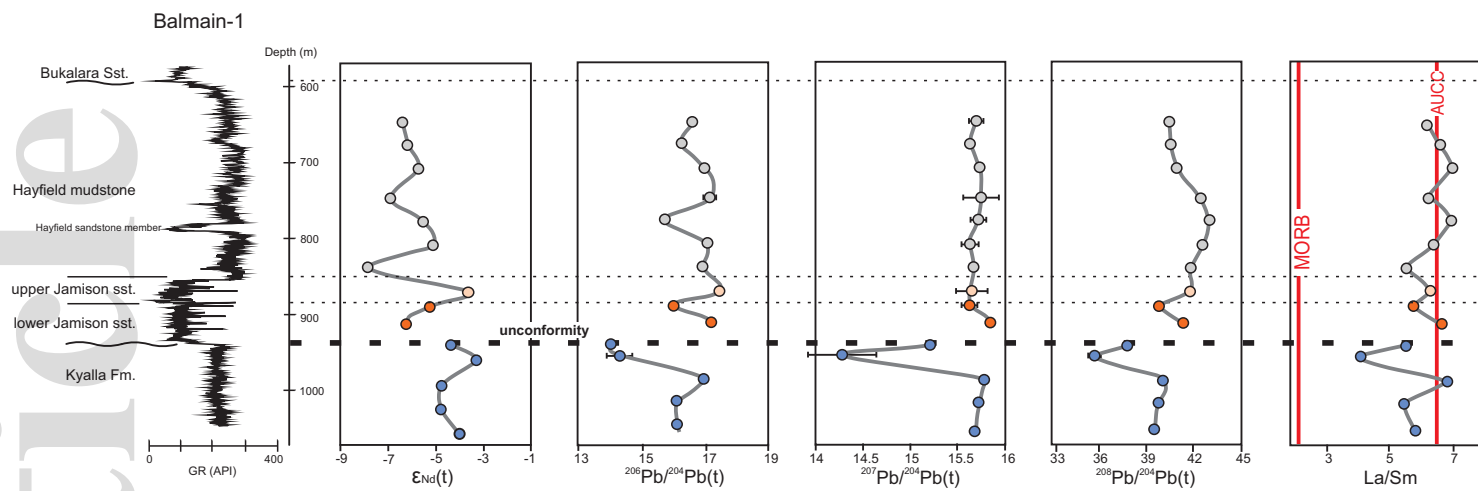
* Pb_c = Total common Pb including analytical blank (0.8 ± 0.3 pg per analysis). ρ = error correlation coefficient of radiogenic

²⁰⁷Pb/²³⁵U vs. ²⁰⁶Pb/²³⁸U. All uncertainties given at 2σ.



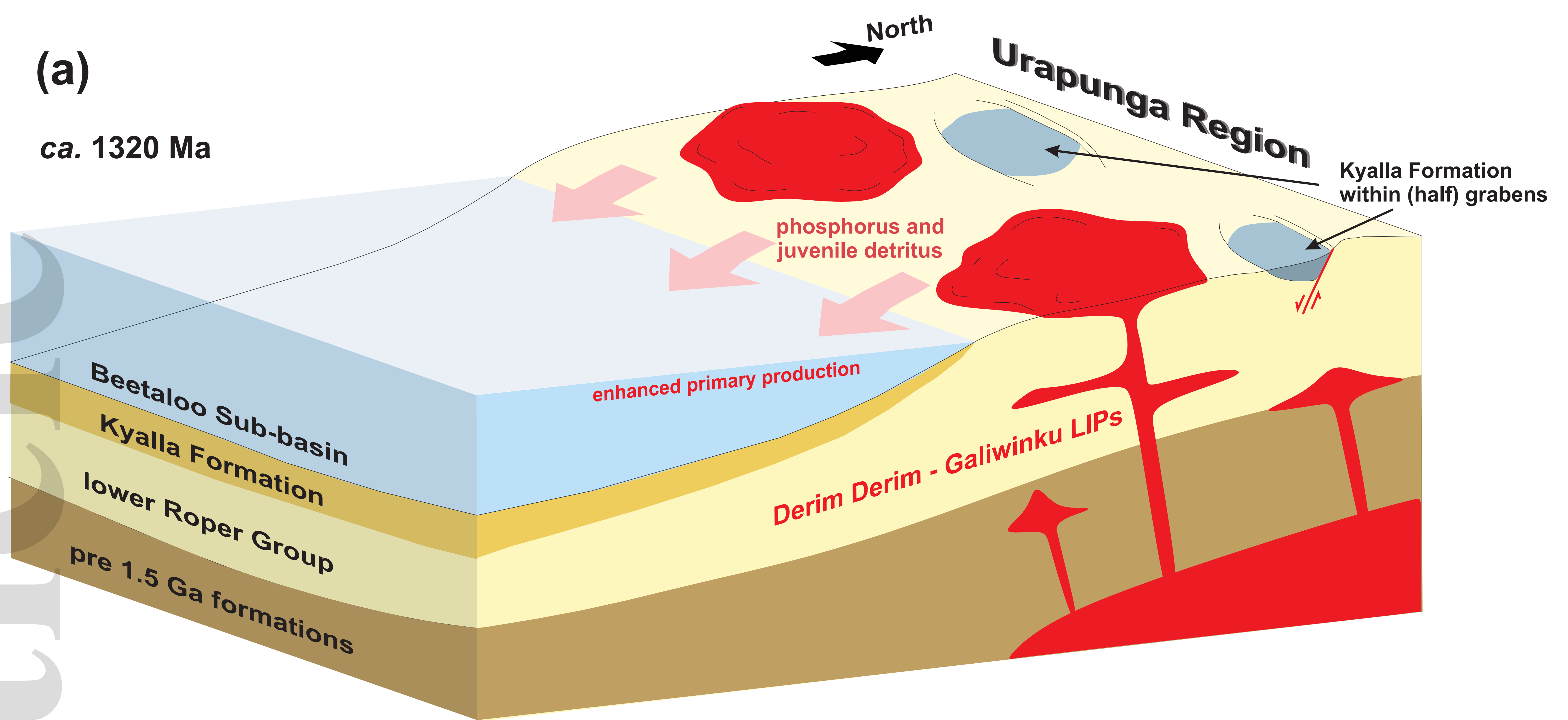






(a)

ca. 1320 Ma



(b)

ca. 1313 Ma

